Song et al. *NPG Asia Materials* (2022) 14:79
https://doi.org/10.1038/s41427-022-00425-0

NPG Asia Materials

ARTICLE Open Access

Engineered magnetic plant biobots for nerve agent removal

Su-Jin Song[1], Carmen C. Mayorga-Martinez[1], Dalibor Huska[1,2] and Martin Pumera[1,2,3,4]

Abstract

Biohybrid micro/nanorobots that integrate biological entities with artificial nanomaterials have shown great potential in the field of biotechnology. However, commonly used physical hybridization approaches can lead to blockages and damage to biological interfaces, impeding the optimal exploitation of natural abilities. Here, we show that magnetically propelled plant biobots (MPBs), employing tomato-callus cultivation engineering in the presence of Fe_3O_4 nanoparticles (NPs), are capable of active movement and directional guidance under a transversal rotating magnetic field. The Fe_3O_4 NPs were transported through the cell growth media and then taken up into the plant tissue cells (PTCs), imparting the plant biobot with magnetic function. Moreover, Fe ions support the growth of callus cells, resulting in nanoparticle incorporation and enabling faster growth and structurally compact texture. The magnetic plant biobots demonstrated rapid and efficient removal of chlorpyrifos (approximately 80%), a hazardous nerve gas agent that causes severe acute toxicity, and recovery using an external magnetic field. The eco-friendly plant biobots described here demonstrate their potential in biomedical and environmental applications.

Introduction

Artificial self-propelled micro/nanorobots are able to perform complex tasks in a wide range of fields[1], such as drug delivery[2–4], biosensing[3,5], and cell manipulation[6,7], as well as numerous water remediation tasks[8–10]. Recently, micro/nanorobots have been studied using various mechanisms and external stimuli, such as light, ultrasound, and magnetic fields[11]. Artificial magnetic micro/nanorobots based on ferromagnetic materials can be propelled by magnetic field, thus providing enhanced functionality such as moving along a driven trajectory[12–14]. Combining self-propulsion with the intrinsic properties of materials, micro/nanorobots can be used for the rapid removal of contaminants such as heavy metal ions and toxic organic compounds[8,14,15].

Organophosphorus (OP) pesticides such as chlorpyrifos, parathion, and malathion are widely used in agriculture to prevent farm products from being damaged by insects[16,17]. Only a small amount of these highly toxic OP pesticides reach their target[18] and the residues accumulate in the environment, thus creating a threat not only to the surrounding environment but also to human and animal health. If accumulated in the human body, chlorpyrifos, one of the most widely used pesticides, can cause dermal irritation, subtle nervous system effects, respiratory distress, and death[19,20]. In addition, the accumulation of pesticides affects the soil half-life and the metabolism of soil microorganisms[21] and has been revealed as one of the main causes of water pollution[22,23]. To reduce damage by chlorpyrifos, a variety of removal and detection[5] methods have been studied.

Magnetically driven micro/nanorobots have been used in biomedical applications and environmental remediation and present advantages such as biocompatibility, remote maneuverability, and versatility and they do not require fuel. Recently, based on these merits, biohybrid micro/nanorobots have been developed in combination

Correspondence: Martin Pumera (pumera.research@gmail.com)
[1]Center for Advanced Functional Nanorobots, Department of Inorganic Chemistry, Faculty of Chemical Technology, University of Chemistry and Technology Prague, Technická 5, 166 28 Prague, Czech Republic
[2]Department of Chemistry and Biochemistry, Mendel University in Brno, Zemedelska 1, 613 00 Brno, Czech Republic
Full list of author information is available at the end of the article

with ferromagnetic nanoparticles (NPs)/structures and natural materials (e.g., cells, bacteria, sperm, pollen, plants, and spores)[24–29]. Biohybrid micro/nanorobots can be operated by diverse propulsion methods, including as chemical, magnetic, and ultrasound techniques[30]. Biohybrid micro/nanorobots that can be propelled by toxic fuels, such as hydrogen peroxide[31], hydrazine[32], and sodium borohydride[33], are limited in their practical applications. Hence, the fabrication of plant-derived biobots combined with plant tissue and ferromagnetic materials is a new direction for biohybrid robots.

In this study, tomato leaf-derived calli were used to fabricate plant robots, and their efficiency of chlorpyrifos removal was investigated. Engineered plant calli were cultivated with Fe_3O_4 NPs and induced magnetic plant biobots (Scheme 1 and Scheme S1). Because the Fe_3O_4 NPs were internalized inside the magnetic plant biobots, it was possible to propel and control them under a transversal rotating magnetic field. The localization of Fe_3O_4 NPs inside the magnetic plant biobots was assessed using scanning electron microscopy (SEM), elemental analysis by energy-dispersive X-ray (EDX), and dark-field microscopy with hyperspectral imaging to obtain further information on Fe_3O_4 NPs within the callus. We demonstrated that the magnetic plant biobots are propelled under magnetic fields without needing toxic chemicals as fuel. In addition, the usability of the magnetic plant biobots was verified by effectively removing chlorpyrifos from the solution. This study focuses on the development of plant-derived biobots and suggests their application for pesticide (chlorpyrifos) removal. The plant-based robots reported here can be propelled under a magnetic field and can efficiently remove pesticides while in motion. In the same vein, magnetic plant biobots can open a new methodology for biohybrid active materials for biomedical and environmental applications.

Results and discussion

Initially, magnetic plant biobots were prepared and characterized. Tomato callus was cultivated on Murashige and Skoog (MS) media[34,35] supplemented with Fe_3O_4 NPs (2 mg/ml) and growth nutrients (6-benzyl aminopurine (BAP) and α-naphthaleneacetic acid (NAA)) as detailed in the Materials and Methods. Tomato callus growth was examined visually for size, pigment, and different concentrations of agar. As shown in Fig. 1A, during 14 days of culture, there was no significant difference in pigmentation and viability of callus cultured with and without Fe_3O_4 NPs. In addition, Fig. S1 shows a comparison of representative digital photographs of callus with and without treatment with Fe_3O_4 NPs. The Fe_3O_4 NP-free callus was brittle compared to the compact texture of the callus cultured with media including Fe_3O_4 NPs[36,37]. These phenomena could be explained by Fe deficiency influencing callus growth during the cultivation period. Fe is an essential element for metabolic reactions in organisms. Fe deficiency in plant callus correlates with its weight, chlorophyll and carotenoid contents, antioxidant enzyme activities, and lipid peroxidation[37]. As proposed in numerous studies, Fe deficiency of the callus induces stress, making it brittle and inhibiting growth, indicating that Fe may be involved in the cell wall structure as observed in the texture of the exposed callus. Fe deficiency also leads to high plant mortality with significant growth inhibition (including yellowing and symptoms of necrosis)[37–40].

In addition, individual callus growth is also affected by the concentration of agar. To optimize the solutions to create magnetic plant biobots, callus was cultivated with Fe_3O_4 NPs and various concentrations of agar (0.4%, 0.6%, 0.8%, and 1.2%). The growth responses of the calli are presented in Fig. 1, Supplementary Fig. S2A–D, and Table S1. As shown in Fig. 1, the average size of the plant calli

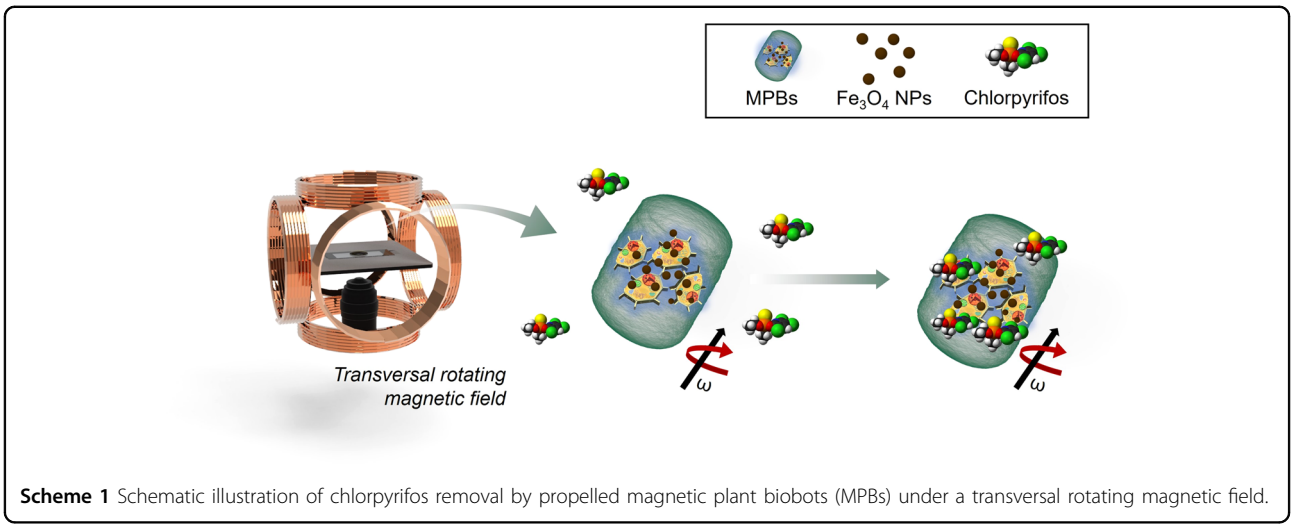

Scheme 1 Schematic illustration of chlorpyrifos removal by propelled magnetic plant biobots (MPBs) under a transversal rotating magnetic field.

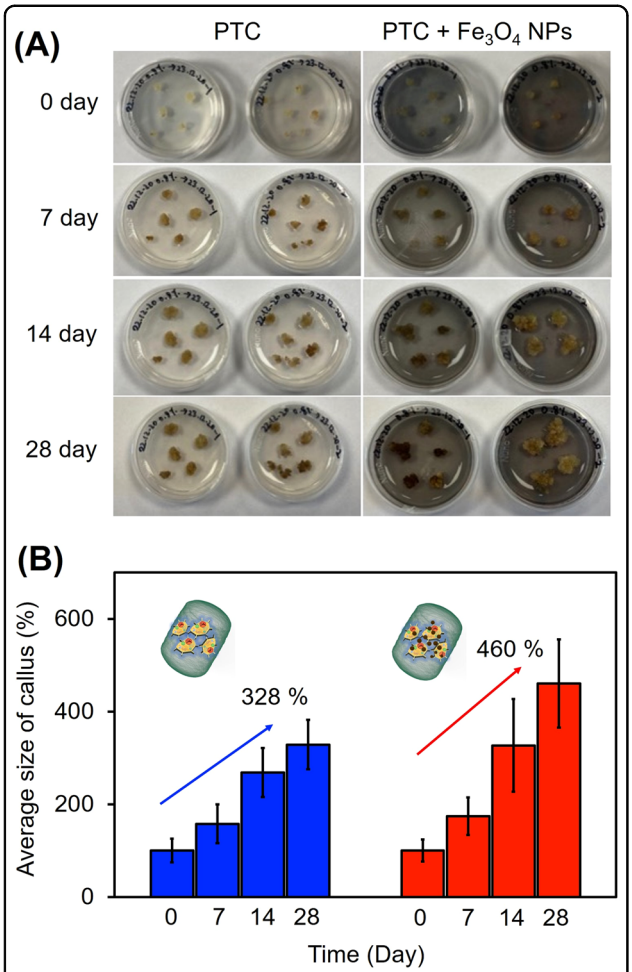

Fig. 1 Plant callus growth on a 0.8% agar plate. A Representative macroscopic images and **B** quantification of the average size of plant calli cultivated with (red column) and without (blue column) Fe_3O_4 NPs for 28 days.

showed no significant difference with or without Fe_3O_4 NPs in the first 7 days, whereas a remarkable each callus size increase was observed in the Fe_3O_4 NP-treated groups after 14 days. After 28 days of cultivation, the mean growth area of callus with Fe_3O_4 NPs (460% ± 95.1 growth compared to the first day) was much larger than that without Fe_3O_4 NPs (328% ± 53.2) (Fig. 1B). The difference in the average size of the calli with and without Fe_3O_4 NPs was ~132%. In addition, to examine the variation in callus growth according to the concentration of agar, calli were cultured on 0.4%, 0.6%, and 1.2% agar plates (Supplementary Fig. S2A–C). The sizes of these calli samples are reported in Table S1. The largest difference in the growth of calli with and without Fe_3O_4 NPs were observed on the 0.6% agar plate, with a difference of ~152%. However, the greatest calli growth were observed on the 0.8% agar plate with Fe_3O_4 NPs (460%) after 28 days (Fig. S2D). Therefore, 0.8% was selected as the optimal agar plate concentration for this study. A similar trend of growth promotion is also observed in Supplementary Fig. S2, suggesting that callus growth was affected by the concentration of agar as well as by the Fe_3O_4 NPs. The optimum concentration and type of agar are important factors in callus growth to avoid the vitrification of callus[41] and decrease the necrosis of plant tissue cells[42], which occur during in vitro plant cell proliferation[43]. In our experiment, the largest and most rigid calli were cultivated on a 0.8% agar plate, whereas calli cultivated on 0.4% and 1.2% agar were unstable and physically brittle, which is in agreement with previous reports[43,44]. Therefore, 0.8% agar was chosen as the optimum concentration for further MPB fabrication. In this study, we confirmed that the appropriate concentration of agar with Fe_3O_4 NPs allowed the magnetic plant biobots to maintain a compact structure and promote the growth of callus for a long-term cultivation period. After 28 days of callus culture in normal media and magnetic plant biobot induction media, distinct differences between plant callus and magnetic plant biobots were observed at both macroscopic and microscopic levels.

Tomato callus cells and magnetic plant biobots were analyzed using SEM. As shown in Fig. 2A, B, the magnetic plant biobots maintained a compact structure compared to the plant callus (without Fe_3O_4 NPs), even after processing by the homogenizer. The existence of Fe_3O_4 NPs in magnetic plant biobots was further confirmed by EDX spectroscopy. EDX elemental mapping confirmed the presence of carbon (C), oxygen (O), and iron (Fe) in the structure of the magnetic plant biobots (Fig. 2C, D and Supplementary Fig. S3). Furthermore, callus cultivated with Fe_3O_4 showed more than 10 times the Fe content in EDX spectroscopy (Supplementary Fig. S3). To further demonstrate the differences in Fe content, inductively coupled plasma–optical emission spectrometry (ICP–OES) was performed (Supplementary Fig. S4). ICP–OES analysis demonstrated that the Fe content in the plant biobots was 0.135 mg/g. However, in plant callus, the content of Fe was 0.021 mg/g. These results indicate that Fe_3O_4 NPs were internalized by plant callus. It should be noted that the Fe content in plant callus is related to the intrinsic Fe that plants need for many biochemical processes from their natural metabolism[36–38].

Hyperspectral imaging combined with dark-field microscopy facilitates the detection and visualization of NPs in biological and environmental fields[45]. To establish the internalization of Fe_3O_4 NPs in cultivated callus, dark-field microscopy with hyperspectral imaging was used to obtain images of callus grown for 28 days in the presence and absence of Fe_3O_4 NPs (Fig. S5A, B). Using hyperspectral imaging, it is easy to distinguish plant cells (green), tissue (no signal), and Fe_3O_4 NPs (yellow). Furthermore, as shown in spectral libraries, it was confirmed

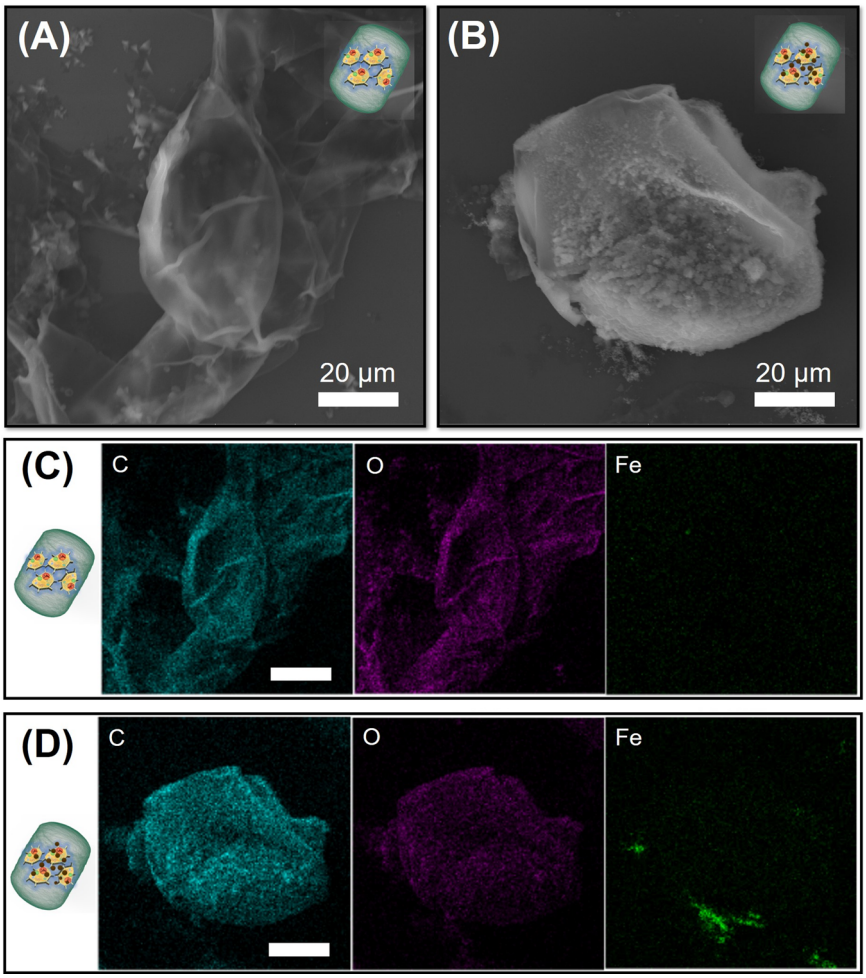

Fig. 2 Scanning electron microscopic analysis. A, **B** SEM images of tomato callus cells (**A**) and magnetic plant biobots (**B**). **C**, **D** EDX mapping of carbon (blue), oxygen (purple), and iron (green) elemental distributions corresponding to tomato callus cells (**C**) and magnetic plant biobots (**D**). Scale bar, 25 μm.

that cells and tissues show absorbance at 400–500 nm, and Fe_3O_4 NPs show absorbance at 700 nm or less. As Fe_3O_4 NPs absorb wavelengths higher than those absorbed by plant cells, this also confirms the presence of Fe_3O_4 NPs. In addition, the morphology and size of the Fe_3O_4 NPs used in callus culture were characterized by transmission electron microscopy (TEM) and EDX spectroscopy (Fig. S6A, B). The elemental mapping micrographs confirm the presence of Fe, O, and C in the Fe_3O_4 NPs. The average size of the Fe_3O_4 NPs was ~150 nm[46], and the size of the final callus was approximately 500 μm. Therefore, it can be considered that the Fe_3O_4 NPs were sufficiently absorbed and internalized into the plant cell during the cultivation period[47,48]. Consequently, these visual data show that the Fe_3O_4 NPs could be effectively taken up by plant callus during the cultivation periods and successfully induce the formation of the plant biobots.

According to previous studies related to nanoparticle–plant cell interactions, the size, surface properties, and concentration of NPs can be crucial factors for the internalization of NPs into plant cells[49–51]. For example, C. Larue et al. demonstrated the internalization of TiO_2 NPs into plant roots. When the different sizes of TiO_2 NPs (14 nm to 665 nm) were exposed to plant roots for 7 days, NPs of less than 140 nm were found in the wheat roots, and NPs of less than 36 nm were found in the parenchyma. Therefore, the uptake of NPs is dependent on their size and the direct interaction between the cell wall components and TiO_2 NPs[51]. In addition, T. Sabo-Attwood et al. also revealed the internalization of NPs within individual plant cells[52]. The results showed that the NPs migrated across the plant cell wall and biomembrane barrier through the presence of clusters in the cytoplasm. Thus, several factors that determine the interaction between NPs and plants have been reported; however, the

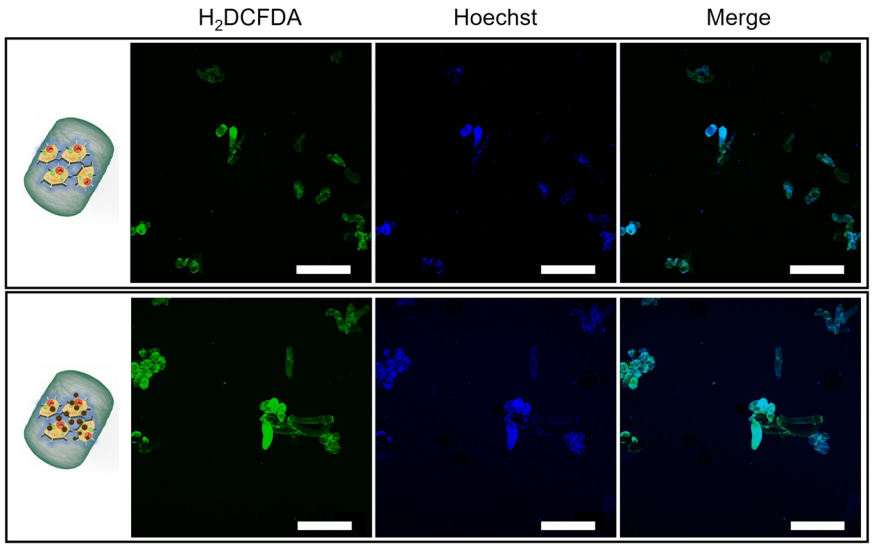

Fig. 3 Effect of Fe_3O_4 NPs on plant callus viability. Fluorescence images by confocal microscopy of plant callus cultivated with (bottom panel) and without (top panel) Fe_3O_4 NPs for 28 days. Plant callus was double-stained with H_2DCFDA and Hoechst to show ROS (green) and nuclei (blue). Scale bar, 500 µm.

exact mechanisms of this interaction have not yet been elucidated.

To evaluate the effect of Fe_3O_4 NPs on callus growth over the culture period, we double-stained cells with H_2DCFDA and Hoechst 33342 and observed the emitted green and blue fluorescence, respectively (Fig. 3). Reactive oxygen species (ROS) are known to have an important role in intracellular mechanisms, such as the delivery of cell signals, apoptosis, and gene expression, in addition to being a stress marker. H_2DCFDA penetrates the cell membrane and infiltrates the cell[53,54]. Here, to examine the nucleic acids, the plant cells were dyed with Hoechst 33342. We observed that both control and treated cells showed a similar pattern and that MPBs can be used for the removal of chlorpyrifos. Furthermore, the samples were analyzed spectrophotometrically for basic stress markers such as carotenoids, total polyphenolics, flavonoids, and antioxidant capacity expressed as EC50 (Fig. S7A–D). In all performed analyses, no significant difference in the content of individual compounds was found. These compounds respond mainly to stress conditions, ROS levels, etc. Under stress conditions, there is an increase in ROS and, thus, an increase in antioxidant compounds. However, as the data show, the samples exposed to Fe_3O_4 NPs did not demonstrate any increase in the abovementioned parameters. These results are consistent with the microscopic analysis, where we observed ROS after H_2DCFDA treatment. Both analyses suggest steady-state and balanced cellular homeostasis in both control and treated cells. Data from samples exposed to NPs show a larger error. This is likely due to the individual NPs not being equally distributed in each cell. These results indicate that the Fe_3O_4 NPs have no negative impact on intra- and extracellular callus.

In addition, the internalization of Fe_3O_4 NPs by MPBs was demonstrated through magnetic actuation and directional control under a transversal rotating magnetic field. Plants absorb Fe ions from the soil[55,56]. However, magnetic motors need ferromagnetic or paramagnetic material to be propelled by the magnetic field[29,57]. Propelled MPBs were evaluated under a transverssal rotating magnetic field using six electromagnetic coils[6]. Video S1 shows the motion of the plant callus and MPBs controlled by magnetic manipulation at a frequency of 2 Hz and a magnetic field intensity of 5 mT in an aqueous solution. Furthermore, Fig. 4 shows the time-lapse tracking line images of plant callus (Fig. 4A) and MPBs (Fig. 4B) in distilled water. The MPBs were sufficiently magnetized to allow rotation with a tumbling motion along the X-Z plane and precise maneuverability under the transversal rotating magnetic field (Video S1). In addition, the controlled guidance of MPBs under rotating magnetic fields was demonstrated by presenting a square propelling path (Video S2). The average velocity of MPBs was 6.023 µm s^{-1} at 2 Hz with 5 mT. However, beyond 2 Hz, MPBs exhibited an unstable state with shaking (Video S3). By integrating biocompatible iron oxides with plant tissue cells, the use of toxic chemical fuels, such as H_2O_2, that potentially can cause damage to weak biological barriers can be avoided.

The comparison of magnetic responsiveness under the transversal rotating magnetic field shown in Video S2 to S3 is direct evidence of Fe_3O_4 NP internalization. When we consider the scale of the callus and NPs (500 µm:

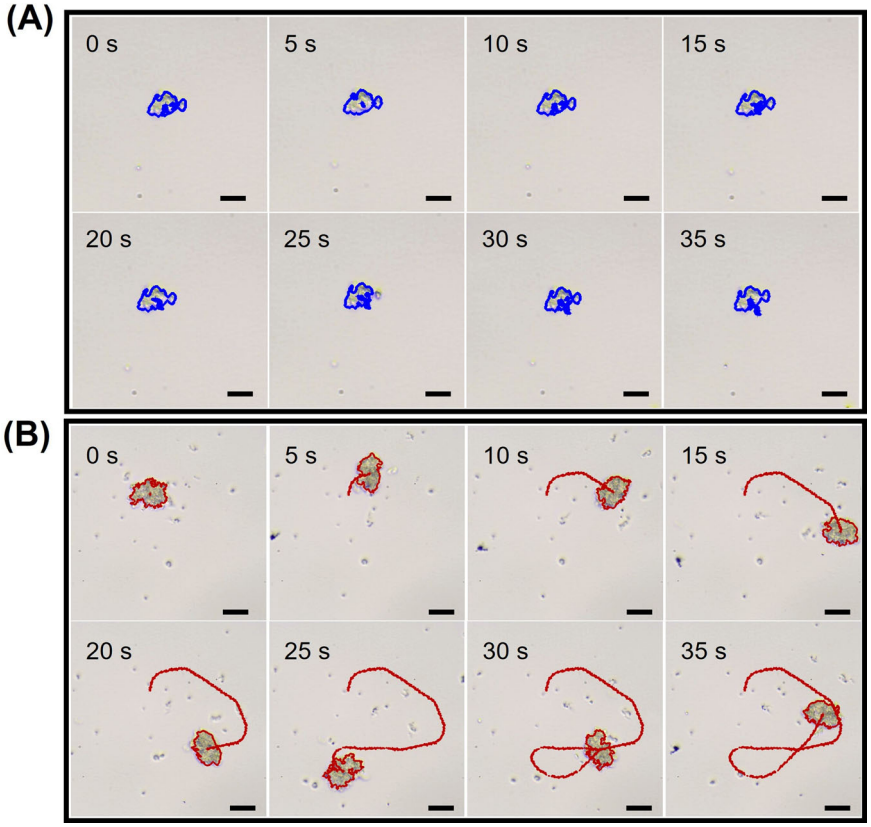

Fig. 4 Time-lapse images of motion behavior of PTCs and MPBs by magnetic manipulation. Motion trajectories of PTCs (**A**) and MPBs (**B**) under a transversal rotating magnetic field within 50 s (2 Hz and 5 mT) (taken from Video S1). Scale bar, 10 μm.

150 nm), this movement likely requires the internalization of many Fe_3O_4 NPs, not just a few. Electron/optical microscopic data support this observation (Figs. 2, S5, and S6). Moreover, the EDX elemental mapping from SEM images (Fig. 2) and ICP–OES analysis (Fig. S4) clearly show the uptake of many Fe_3O_4 NPs. In EDX images, the green area that corresponds to the Fe element is more than 25 μm in length.

After the efficient magnetic propulsion of the biobots was demonstrated, nerve agent (chlorpyrifos) removal was performed *via* a magnetic manipulation, and the performance of the magnetic plant biobots was compared to that of the plant callus without Fe_3O_4 NPs (static mode). We demonstrated chlorpyrifos removal by PTCs and MPBs using programmed random mode propulsion, and the amount of chlorpyrifos was quantified by the calibration curves shown in Fig. S8A–C. Figure 5 shows that chlorpyrifos was efficiently removed by the actively moved magnetic plant biobots as a function of time. According to Fig. 5A, C, the final residual chlorpyrifos after exposure to plant callus and magnetic plant biobots was measured to be 3 ppm and 0.3 ppm, respectively. With the activation of MPBs, the chlorpyrifos removal efficiency reached >60% within only 30 min (Fig. 5B). Most of the removal was achieved after 180 min, when the removal efficiency was 80% and 64% for the magnetic plant biobots and plant callus, respectively, suggesting that the performance of dynamic MPBs was ~20% more efficient than that of static plant callus (Fig. 5D). The main advantage of our motors, apart from functioning as mobile microcleaners, is the possibility of extracting the pesticide by the retrieval of MPBs using an external magnet (see Video S4), which we cannot do with simple tomato cells. Moreover, the MPBs were readily separated by an external permanent magnet, which can be utilized for the recovery of the MPBs after chlorpyrifos removal (Video S4 and Fig. S9A, B). Consequently, by exploiting the nature of plant callus cells and dynamic motion along with magnetically guided control and facile recovery, we demonstrated for the first time the ability of high-performance plant biobots to successfully remove chlorpyrifos from plant cells.

The uptake of pesticides (i.e., organic chemicals) into plants could be facilitated through three major pathways: dispersal into various parts of plants through root uptake, absorption from the surrounding atmosphere, or diffusion through the plant surface due to contaminants deposited

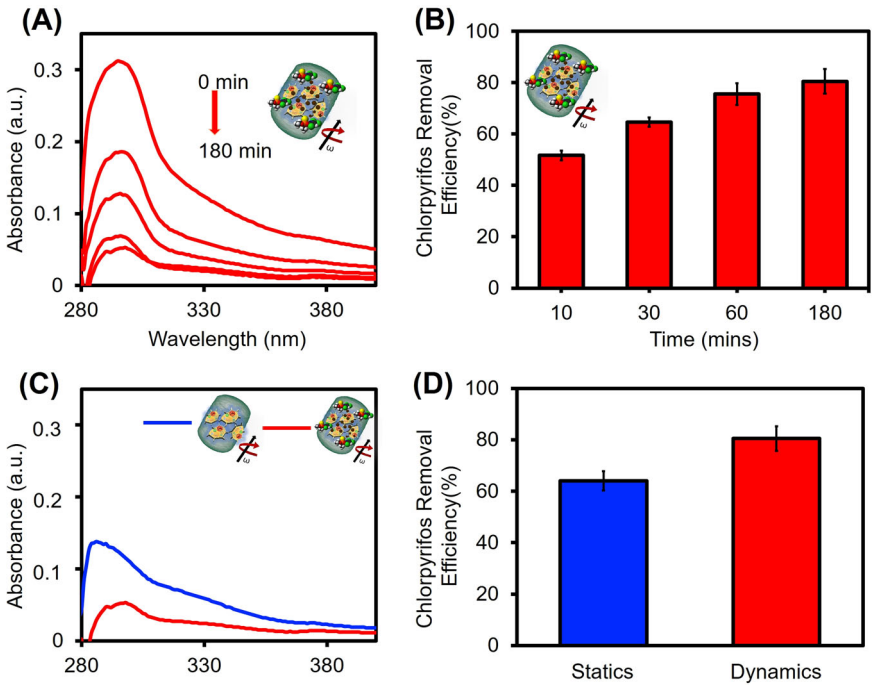

Fig. 5 Nerve agent (chlorpyrifos) removal performance by MPBs. UV–Vis absorption spectra of chlorpyrifos removal over the time by MPBs (**A**), chlorpyrifos removal percentage in a time-dependent manner (**B**), UV–Vis absorption spectra of chlorpyrifos removal by MPBs (red line) and PTCs (blue line) (**C**), and comparison of chlorpyrifos removal percentage by using PTCs (blue column) and MPBs (red column) after 180 min of treatment (**D**).

on the plant epidermis[58,59]. Pesticides absorbed from the soil can be localized within plant tissue or dispersed to other plant regions through vascular bundles. Previous studies of the uptake of organic chemicals into plants have shown that these chemicals flow into plants mainly through passive and diffusive processes[60]. Translocation of pesticides within the plants penetrates multiple layers, including the epidermis, cortex, endodermis, and pericycle, through the xylem. This flow is operated by the water potential gradient created throughout the plant[61]. Therefore, the plant uptake process can depend on the enzyme activity in specific plant tissues and the environmental variables.

Conclusions

In this work, the removal of the pesticide chlorpyrifos was demonstrated using plant-based robots. To produce magnetic plant biobots, we cultivated plant calli on media containing ferromagnetic material (Fe_3O_4 NPs). The Fe_3O_4 NPs were taken up inside the plant cells during their growth. Moreover, Fe_3O_4 NPs were not toxic to plant calli, providing structural stability and enhancing callus growth. The plant-based robots had a growth rate of 460% and excellent removal efficiency of 80% for chlorpyrifos. The great advantage of these magnetic plant biobots is their simple preparation. This procedure can be easily scaled up. These results suggest that magnetic plant biobots can be effectively used not only for pesticide removal but also for heavy metal removal. Furthermore, magnetic plant biobots are excellent candidates to remediate polluted water.

Materials and methods

Seed germination and callus induction

Several leaves from well-grown tomatoes were carefully cut to an approximately uniform shape using a sterile scalpel blade. For surface sterilization, leaf explants were immersed in 70% ethanol for 1 min and 2.5% (v/v) sodium hypochlorite for 5 min and then washed three times with distilled water. Seeds of tomato thus prepared were germinated in 1/2 MS media consisting of 1% sucrose and 0.7% agar on a petri dish at 22–24 °C under dark conditions. For callus induction, germinated seeds were inoculated in semisolid MS media with phytohormones such as NAA and BAP, and callus was obtained after a few weeks.

Cultivation of plant callus

Callus cultivation was accomplished in two different media conditions, i.e., MS media supplemented with NAA (auxin), BAP (cytokinin), and 3% sucrose in the presence/absence of Fe_3O_4 NPs. To induce the plant biobots, Fe_3O_4

NPs (2 mg/mL) were mixed with MS media by an ultrasound probe. Both media were solidified with four different concentrations of agar (0.4%, 0.6%, 0.8%, and 1.2%). After the explants were cultivated in two different types of media (with and without Fe_3O_4 NPs), their size and morphology were recorded weekly, and the data were analyzed using a digital camera and ImageJ software.

Characterization of PTC

Tomato callus cells and magnetic plant biobots were examined by SEM (MAIA3 Tescan) with affiliated EDX (Oxford) spectroscopy and hyperspectral microscopy (CytoViva Inc., USA) analysis. For analysis, the callus samples were fixed in 5% glutaraldehyde in 0.1 M PBS (pH 7.2) for 2 h at room temperature. Samples were washed with distilled water and dehydrated in a graded ethanol series (40%, 50%, 60%, 70%, 80%, and 90%) for 15 min each and then placed in 100% ethanol for 10 min. Finally, the samples were completely dried. To compare the Fe content of the samples, inductively coupled plasma–optical emission spectrometry (ICP–OES, Spectro Arcos) was used.

Plant tissue cell compatibility with Fe_3O_4 NPs

To evaluate the effects of Fe_3O_4 NPs on plant callus and magnetic plant biobots, samples were treated with H_2DCFDA and Hoechst 33342. Each sample was washed with PBS before adding the working solution. The ROS levels in the PTCs were evaluated by staining with the 10 μM fluorescent probe 2'7'-dichlorodihydrofluorescein diacetate (H_2DCFDA) and incubating at 37 °C in the dark. For nuclear staining, Hoechst 33342 (10 μg/mL) was added before the end of the reaction time of H_2DCFDA. Samples were then washed twice before imaging by confocal microscopy (ZEISS LSM 880). H_2DCFDA fluorescence was determined at Ex_{492}/Em_{525}. The resolution was set to 792 × 792. 40× magnification was used for visualization.

Spectrophotometric analysis

Determinations of phenolic compounds, flavonoids, carotenoids, and antioxidant activity were based on a previous experiment[62]. Samples were homogenized at 15,000 rcf (Precellys Evolution Homogenizer, Bertin-Instruments, France) and then measured by a spectrophotometer (Infinite M200 Pro, Tecan, Männedorf, Switzerland with Tecan i-control software, 1.9).

Motion studies of magnetic plant biobots

Motion studies of magnetic plant biobots were conducted on rotating magnetic manipulation systems. The magnetic plant biobots were mixed well with distilled water and dropcast onto a glass slide. The samples were recorded as 50-second videos at 30 frames per second. The movement of the magnetic plant biobots was observed by optical microscopy using a high-resolution camera, and the videos were analyzed through a computer system.

Chlorpyrifos removal

To evaluate the pesticide removal efficiency of the magnetic plant biobots, chlorpyrifos was employed, which is the most commonly used pesticide in agriculture. Briefly, part of the isolated plant callus and magnetic plant biobots were added to 10 ppm chlorpyrifos solution under a rotating magnetic field at room temperature for 3 h. The supernatant of the working solution was collected at constant time intervals by centrifugation and measured by absorbance from 200 to 800 nm using UV–Vis spectroscopy. The removal efficiency of chlorpyrifos was calculated as follows:

$$\text{Removal efficiency}(\%) = \frac{C_0 - C_1}{C_0} \times 100$$

where C_0 is the initial concentration of the chlorpyrifos solution and C_1 is the concentration of the chlorpyrifos solution after removal. The concentrations of chlorpyrifos and callus were also determined by UV–Vis spectroscopy.

Statistical analysis

The software R 3.3.2 and RStudio Desktop for Windows (RStudio Team (2020)) were used in the analysis. RStudio: Integrated Development for R (RStudio, PBC, Boston, MA, URL http://www.rstudio.com/) was used for statistical calculations. Mean values for individual treatments were compared with mean values of unexposed controls using the post hoc Tukey test. Mean values ($n = 3$). The results are expressed as the mean ± standard deviation.

Acknowledgements

This work was supported by the project Advanced Functional Nanorobots (reg. no. CZ.02.1.01/0.0/0.0/15_003/0000444 financed by the EFRR).

Author details

[1]Center for Advanced Functional Nanorobots, Department of Inorganic Chemistry, Faculty of Chemical Technology, University of Chemistry and Technology Prague, Technická 5, 166 28 Prague, Czech Republic. [2]Department of Chemistry and Biochemistry, Mendel University in Brno, Zemedelska 1, 613 00 Brno, Czech Republic. [3]Future Energy and Innovation Laboratory, Central European Institute of Technology, Brno University of Technology, Purkynova 656/123, Brno CZ-616 00, Czech Republic. [4]Department of Medical Research, China Medical University Hospital, China Medical University, No. 91 Hsueh-Shih Road, Taichung, Taiwan

Author contributions

M.P., C.C.M.-M., D.H., and S.J.S. devised and planned the experiments; S.J.S. performed the cultivation of plant callus, plant biobot motion study, and pesticide removal experiments, and wrote original draft; D.H. carried out plant callus preparation and analysis of fluorescence images; C.C.M.-M. was responsible for formal analysis, supervision, and manuscript revision; M.P. originated the idea and was in charge of project development.

Competing interests
The authors declare no competing interests.

Publisher's note
Springer Nature remains neutral with regard to jurisdictional claims in published maps and institutional affiliations.

Supplementary information The online version contains supplementary material available at https://doi.org/10.1038/s41427-022-00425-0.

Received: 13 January 2022 Revised: 31 July 2022 Accepted: 3 August 2022.
Published online: 30 September 2022

References

1. Parmar, J., Vilela, D., Villa, K., Wang, J. & Sánchez, S. Micro-and nanomotors as active environmental microcleaners and sensors. *J. Am. Chem. Soc.* **140**, 9317–9331 (2018).
2. Tang, S., et al. Enzyme-powered janus platelet cell robots for active and targeted drug delivery. *Sci. Robot.* **5**, No. eaba6137 (2020).
3. Agrahari, V. et al. Intelligent micro-/nanorobots as drug and cell carrier devices for biomedical therapeutic advancement: promising development opportunities and translational challenges. *Biomaterials* **260**, 120163 (2020).
4. Chen, X.-Z. et al. Hybrid magnetoelectric nanowires for nanorobotic applications: fabrication, magnetoelectric coupling, and magnetically assisted in vitro targeted drug delivery. *Adv. Mater.* **29**, 1605458 (2017).
5. Ergeneman, O. et al. In vitro oxygen sensing using intraocular microrobots. *IEEE Trans. Biomed. Eng.* **59**, 3104–3109 (2012).
6. Vyskocil, J. et al. Cancer cells microsurgery via asymmetric bent surface Au/Ag/Ni microrobotic scalpels through a transversal rotating magnetic field. *ACS Nano* **14**, 8247–8256 (2020).
7. Koleoso, M. et al. Micro/nanoscale magnetic robots for biomedical applications. *Mater. Today Bio* **8**, 100085 (2020).
8. Ying, Y., Pourrahimi, A. M., Sofer, Z., Matějková, S. & Pumera, M. Radioactive uranium preconcentration via self-propelled autonomous microrobots based on metal–organic frameworks. *ACS Nano* **13**, 11477–11487 (2019).
9. Novotny, F., Wang, H. & Pumera, M. Nanorobots: machines squeezed between molecular motors and micromotors. *Chem* **6**, 867–884 (2020).
10. Wang, J. *Nanomachines: Fundamentals and Applications*. (Wiley-VCH, Weinheim, Germany, 2013).
11. Gao, W. & Wang, J. The environmental impact of micro/nanomachines: a review. *ACS Nano* **8**, 3170–3180 (2014).
12. Wang, B. et al. Reconfigurable swarms of ferromagnetic colloids for enhanced local hyperthermia. *Adv. Funct. Mater.* **28**, 1705701 (2018).
13. Mahoney, A. W., Nelson, N. D., Peyer, K. E., Nelson, B. J. & Abbott, J. J. Behavior of rotating magnetic microrobots above the step-out frequency with application to control of multi-microrobot systems. *Appl. Phys. Lett.* **104**, 144101 (2014).
14. Park, J., Jin, C., Lee, S., Kim, J. Y. & Choi, H. Magnetically actuated degradable microrobots for actively controlled drug release and hyperthermia therapy. *Adv. Healthc. Mater.* **8**, 1900213 (2019).
15. Zhou, H., Mayorga-Martinez, C. C., Pané, S., Zhang, L. & Pumera, M. Magnetically driven micro and nanorobots. *Chem. Rev.* **121**, 4999–5041 (2021).
16. Govindasamy, M. et al. Nanocomposites composed of layered molybdenum disulfide and graphene for highly sensitive amperometric determination of methyl parathion. *Microchim. Acta* **184**, 725–733 (2017).
17. Yadav, M., Shukla, A. K., Srivastva, N., Upadhyay, S. N. & Dubey, S. K. Utilization of microbial community potential for removal of chlorpyrifos: a review. *Crit. Rev. Biotechnol.* **36**, 727–742 (2016).
18. Pimentel, D. Amounts of pesticides reaching target pests: environmental impacts and ethics. *J. Agric. Environ. Ethics* **8**, 17–29 (1995).
19. Ma, P. et al. Rapid quantitative determination of chlorpyrifos pesticide residues in tomatoes by surface-enhanced raman spectroscopy. *Eur. Food Res. Technol.* **246**, 239–251 (2020).
20. Wang, P. et al. Visible light photoelectrochemical sensor based on au nanoparticles and molecularly imprinted poly (o-phenylenediamine)-modified TiO 2 nanotubes for specific and sensitive detection chlorpyrifos. *Analyst* **138**, 939–945 (2013).
21. Eisler, R. *Handbook of Chemical Risk Assessment*: Health Hazards to Humans, Plants, and Animals (Volume 1, Lewis Publisher, Boca Raton, RL 2000).
22. Tariq, M. I., Afzal, S., Hussain, I. & Sultana, N. Pesticides exposure in pakistan: a review. *Environ. Int.* **33**, 1107–1122 (2007).
23. McKnight, U. S., Rasmussen, J. J., Kronvang, B., Binning, P. J. & Bjerg, P. L. Sources, occurrence and predicted aquatic impact of legacy and contemporary pesticides in streams. *Environ. Pollut.* **200**, 64–76 (2015).
24. Wang, Q. & Zhang, L. External power-driven microrobotic swarm: from fundamental understanding to imaging-guided delivery. *ACS Nano* **15**, 149–174 (2021).
25. Wang, H. & Pumera, M. Micro/nanomachines and living biosystems: from simple interactions to microcyborgs. *Adv. Funct. Mater.* **28**, 1705421 (2018).
26. Magdanz, V. et al. IRONSperm: sperm-templated soft magnetic microrobots. *Sci. Adv.* **6**, eaba5855 (2020).
27. Zhang, Y. et al. Real-time tracking of fluorescent magnetic spore–based microrobots for remote detection of C. diff toxins. *Sci. Adv.* **5**, eaau9650 (2019).
28. Huska, D., Mayorga-Martinez, C. C., Zelinka R. & Pumera M. Mangetic biohybrid robots as efficient drgu carrier to generate plant cell clones. *Small* (e-pub ahead of print 10 May 2022; https://doi.org/10.1002/small.202200208).
29. Yasa, I. C., Ceylan, H., Bozuyuk, U., Wild, A.-M. & Sitti, M. Elucidating the interaction dynamics between microswimmer body and immune system for medical microrobots. *Sci. Robotics* **5**, eaaz3867 (2020).
30. Soto, F. et al. Smart materials for microrobots. *Chem. Rev.* **122**, 5365–5403 (2021).
31. Safdar, M., Wani, O. M. & Jänis, J. Manganese oxide-based chemically powered micromotors. *ACS Appl. Mater. Interfaces* **7**, 25580–25585 (2015).
32. Gao, W., Pei, A., Dong, R. & Wang, J. Catalytic iridium-based janus micromotors powered by ultralow levels of chemical fuels. *J. Am. Chem. Soc.* **136**, 2276–2279 (2014).
33. Srivastava, S. K., Guix, M. & Schmidt, O. G. Wastewater mediated activation of micromotors for efficient water cleaning. *Nano Lett.* **16**, 817–821 (2016).
34. Murashige, T. & Skoog, F. A revised medium for rapid growth and bioassays with tabacco tissue culture. *Physiol. Plant.* **15**, 473–497 (1962).
35. Zhang, K. et al. A common wild rice-derived BOC1 allele reduces callus browning in indica rice transformation. *Nat. Commun.* **1**, 1–15 (2020).
36. Vigani, G. et al. Three-dimensional reconstruction, by TEM tomography, of the ultrastructural modifications occurring in *Cucumis sativus* L. mitochondria under Fe deficiency. *PLoS One* **10**, e0129141 (2015).
37. Boamponsem, G. A., Leung, D. W. & Lister, C. Relationships among iron deficit-induced potato callus growth inhibition, fe distribution, chlorosis, and oxidative stress amplified by reduced antioxidative enzyme activities. *Plant Cell Tissue Organ Cult.* **132**, 393–412 (2018).
38. Gruber, B. & Kosegarten, H. Depressed growth of non-chlorotic vine grown in calcareous soil is an iron deficiency symptom prior to leaf chlorosis. *J. Plant. Nutr. Soil Sci.* **165**, 111–117 (2002).
39. de laGuardia, M. D. & Alcántara, E. Bicarbonate and low iron level increase root to total plant weight ratio in olive and peach rootstock. *J. Plant Nutr.* **25**, 1021–1032 (2002).
40. Boamponsem, G. A. & Leung, D. W. Use of compact and friable callus cultures to study adaptive morphological and biochemical responses of potato (Solanum tuberosum) to iron supply. *Sci. Hortic.* **219**, 161–172 (2017).
41. Ghashghaie, J., Brenckmann, F. & Saugier, B. Effects of agar concentration on water status and growth of rose plants cultured in vitro. *Physiol. Plant.* **82**, 73–78 (1991).
42. Debergh, P. C. Effects of agar brand and concentration on the tissue culture medium. *Physiol. Plant.* **59**, 270–276 (1983).
43. Kadota, M. & Niimi, Y. Effect of cytokinin types and their concentrations on shoot proliferation and hyperhydricity in in vitro pear cultivar shoots. *Plant Cell Tissue Organ Cult.* **72**, 261–265 (2003).
44. Beaudoin, N., Serizet, C., Gosti, F. & Giraudat, J. Interactions between abscisic acid and ethylene signaling cascades. *Plant Cell* **12**, 1103–1115 (2000).
45. Fakhrullin, R., Nigamatzyanova, L. & Fakhrullina, G. Dark-field/hyperspectral microscopy for detecting nanoscale particles in environmental nanotoxicology research. *Sci. Total Environ.* **772**, 145478 (2021).
46. Kim, J., Mayorga-Martinez, C. C., Vyskocil, J., Ruzek, D. & Pumera, M. Plasmonic-magnetic nanorobots for SAS-CoV-2 RNA detection through electronic readout. *Appl. Mater. Today* **27**, 101402 (2022).
47. Ma, X., Geiser-Lee, J., Deng, Y. & Kolmakov, A. Interactions between engineered nanoparticles (ENPs) and plants: phytotoxicity, uptake and accumulation. *Sci. Total Environ.* **408**, 3053–3061 (2010).

48. Lin, S. et al. Uptake, translocation, and transmission of carbon nanomaterials in rice plants. *Small* **5**, 1128–1132 (2009).
49. Sun, D. et al. Uptake and cellular distribution, in four plant species, of fluorescently labeled mesoporous silica nanoparticles. *Plant Cell Rep.* **33**, 1389–1402 (2014).
50. Avellan, A. et al. Nanoparticle size and coating chemistry control foliar uptake pathways, translocation, and leaf-to-rhizosphere transport in wheat. *ACS Nano* **13**, 5291–5305 (2019).
51. Larue, C. et al. Translocation and Impact of TiO_2 nanoparticles in wheat (triticum aestivum spp.): influence of diameter and crystal phase. *Sci. Total Environ.* **431**, 197–208 (2012).
52. Sabo-Attwood, T. et al. Uptake, distribution and toxicity of gold nanoparticles in tobacco (nicotiana xanthi) seedlings. *Nanotoxicology* **6**, 353–360 (2012).
53. Lyublinskaya, O. et al. Redox environment in stem and differentiated cells: a quantitative approach. *Redox Biol.* **12**, 758–769 (2017).
54. Ravindran, R. et al. The amino acid sensor GCN2 controls gut inflammation by inhibiting inflammasome activation. *Nature* **531**, 523–527 (2016).
55. Arif, N. et al. Influence of high and low levels of plant-beneficial heavy metal ions on plant growth and development. *Front. Environ. Sci.* **4**, 69 (2016).
56. Jin, C. W. et al. Elevated carbon dioxide improves plant iron nutrition through enhancing the iron-deficiency-induced responses under iron limited conditions in tomato. *Plant Physiol.* **150**, 272–280 (2009).
57. Jin, D. & Zhang, L. Collective behaviors of magnetic active matter: recent progress toward reconfigurable, adaptive, and multifunctional swarming micro/nanorobots. *Acc. Chem. Res.* **55**, 98–109 (2021).
58. Burken, J. Uptake and Metabolism of Organic Compounds: Green-Liver Model. In *Phytoremediation: Transformation and Control of Contamina*nts (ed. McCutcheon, S.C., Schnoor, J. L.) pp. 59–84 (John Wiley & Sons, Inc.: Hoboken, NJ, USA 2003).
59. Svobodová, M., Šmídová, K., Hvězdová, M. & Hofman, J. Uptake kinetics of pesticides chlorpyrifos and tebuconazole in the earthworm eisenia andrei in two different soils. *Environ. Pollut.* **236**, 257–264 (2018).
60. Su, Y. & Liang, Y. Foliar uptake and translocation of formaldehyde with bracket plants (Chlorophytum comosum). *J. Hazard. Mater.* **291**, 120–128 (2015).
61. Collins, C., Fryer, M. & Grosso, A. Plant uptake of non-ionic organic chemicals. *Environ. Sci. Technol.* **40**, 45–52 (2006).
62. Kolackova, M. et al. Lycorine and UV-C stimulate phenolic secondary metabolites production and MiRNA expression in Chlamydomonas reinhardtii. *J. Hazard. Mater.* **391**, 122088 (2020).